Solar Physics (2006) 236: 293–311
DOI: 10.1007/s11207-006-0050-4

ON THE TEMPORAL AND SPATIAL PROPERTIES OF ELEMENTARY BURSTS

JIONG QIU[1,2,†] and HAIMIN WANG[1,3]
[1]*Big Bear Solar Observatory, New Jersey Institute of Technology, 40386 N. Shore Ln, Big Bear City, CA 92314-9672, U.S.A.*
[2]*Division of Physics, Mathematics, and Astronomy, California Institute of Technology, MS106-38, 1200 E. California Blvd., Pasadena, CA 91125, U.S.A.*
[3]*Center for Solar Research, Physics Department, New Jersey Institute of Technology, 323 ML King Blvd., Newark, NJ 07102-1982, U.S.A.*

(Received 17 August 2005; accepted 8 May 2006)

Abstract. "Elementary bursts" refer to fine time structures on scales of tens of milli-second to a few seconds in flare radiations. In this paper, we investigate temporal and spatial properties of elementary bursts by exploiting high-cadence Hα (100 ms) and hard X-ray (125 – 500 ms) observations of an impulsive flare on March 16, 2000. We find that the time scale of 2 – 3 s is likely an upper limit of the elementary bursts in this event, at which hard X-ray emissions observed by different instruments correlate, low energy ($\leq$30 keV) hard X-rays and Hα flux correlate, and Hα emissions at conjugate flare kernels correlate. From our methods, and also largely limited by instrument resolutions, there is a weak indication of existence of sub-second structures. With the high-resolution Hα data, we also attempt to explore the spatial structure of "elementary bursts" by determining the average spatial displacement of Hα peak emission between successive "elementary bursts" defined from hard X-ray light curves. We find that, at the time scale of 3 s, the smallest spatial scale, as limited by the imaging resolution, is about $0.4''$. We discuss these results with respect to mechanisms of fragmented magnetic energy release.

1. Introduction

It was first discovered in high-resolution hard X-ray and microwave observations that flare bursts consist of fine structures on time scales from tens of milli-seconds to a few seconds (van Beek, de Feiter, and de Jager, 1974, 1976; Hoyng, van Beek, and Brown, 1976; Kiplinger *et al.*, 1983, 1988; Kaufmann *et al.*, 1980, 1984, 2001; Aschwanden, Benz, and Schwartz, 1993; Aschwanden, Schwartz, and Alt, 1995; Aschwanden *et al.*, 1995, 1998). These are called "elementary bursts" (de Jager and de Jonge, 1978). In recent years, effort to search for small scale structures has also been made in optical wavelengths, typically Hα observations (Wang *et al.*, 2000; Trottet *et al.*, 2000; Kurt *et al.*, 2000). These high-cadence optical observations are exploited to study the elementary bursts because of their good spatial resolution, with which we can hopefully determine some spatial properties of elementary bursts. For example, Wang *et al.* (2000) reported fine temporal structures

[†]Present address: Physics Department, Montana State University, Bozeman MT 59717-3840 (e-mail: qiuj@solar.physics.montana.edu).

of order 300 – 700 ms in Hα off-band emission, and found that these fine structures only occur at flare kernels whose light curves are well correlated with hard X-ray emission. These observations confirm that flare energy release is fragmented.

Understanding the cause of fragmentation is important as it directly points to the nature of flare energy release. From the theoretical point of view, there exist two contrasting scenarios on the scales of energy release. From the magnetohydrodynamic (MHD) point of view, magnetic reconnection and formation of electric current sheets occur at macroscopic scales, as has been manifested by accumulating observations of progressive magnetic reconnection in dynamic two-ribbon flares (Švestka, 1976). Existence of the macroscopic electric current sheet conveniently provides a mechanism to directly accelerate electrons and heat flare plasmas simultaneously (Holman, 1985; Benka and Holman, 1994).

On the other hand, discovery of fine temporal structures in flares leads scientists to consider that magnetic energy release primarily occurs on small scales. Lu and Hamilton (1991) proposed that the coronal magnetic fields are in a self-organized critical state, and solar flares are avalanches of many small scale events. In their *ad hoc* cellular automaton model, only one scale, which is determined by the minimum size of energy dissipation, is meaningful, while flares of different sizes are due to different numbers of such small events. In terms of the physical mechanisms, the most popular belief is that solar flares comprise many small scale reconnections (Sturrock *et al.*, 1984; Parker, 1989; Bastian and Valhos, 1997). LaRosa and Moore (1993) proposed another mechanism that the MHD turbulent cascade rapidly dissipates the bulk kinetic energy of the outflows from many separate reconnection events. According to both models, the lower limit of the time scale depends on the characteristic size of the elementary flux tube. From a different point of view, it has been discussed that along the length of the pre-reconnection current sheet, a tearing mode instability may occur to trigger reconnection and form magnetic islands (Furth, Killeen, and Rosenbluth, 1963), the size and periodicity of which determine the properties of the observed structures. Formation of magnetic islands by tearing-instabilities and subsequent interactions between these magnetic islands, namely the dynamic magnetic reconnection (Kliem *et al.*, 2000 and references therein), are considered to account for fast variations in non-thermal emissions on "elementary burst" timescales (Aschwanden, 2002 and references therein).

In reality, during magnetic energy release in a flare, it is difficult to clearly separate different physical mechanisms that control the scales of energy release. However, it is possible that different mechanisms are characterized by differing time scales and properties, such as periodicity, so that it is still meaningful to discuss what physical mechanism dominates a specific time and spatial scale. With the ever advancing resolving capability of the observing instruments, in the near future, determination of the spatial scales corresponding to the time scales will greatly help elucidate the physical picture of the flare energy release.

Since 1999 August, Big Bear Solar Observatory (BBSO) has carried out a high cadence flare-watch campaign. A Silicon Mountain Design (SMD) high frame rate

CCD camera is mounted on the 26-inch telescope with an image acquisition rate of up to 30 frames per second. The observing wavelength is usually tuned at 1.3 Å in the blue wing of Hα line using a Zeiss filter with the bandpass of 0.25 Å. We look at the far blue wing of the Hα line in an attempt to locate sites of non-thermal beam precipitation in the impulsive phase of solar flares. The campaign has yielded fruitful results in the high resolution study of flares and related phenomena (Wang *et al.*, 2000; Qiu *et al.*, 2000, 2001, 2002; Ding *et al.*, 2001; Wang and Qiu, 2002). In this paper, we proceed with the investigation of fine structures of solar flares using both Hα and hard X-ray observations with the highest available resolutions.

The flare event studied in the present paper was observed on March 16, 2000 by BBSO and *Yohkoh* (Ogawara *et al.*, 1991). This intriguing C9.0 impulsive flare was extensively studied by Qiu *et al.* (2001, 2002). Qiu *et al.* (2002) studied the aspect of the flare Hα kernel motion which was used to infer the macroscopic electric field generated inside the reconnecting current sheets at the coronal reconnecting site. This paper is intended to explore the microscopic aspect of the same flare event as complementary to the study by Qiu *et al.* (2002). Specifically, based on available observations, we address the following issues: (1) the characteristic time scale of elementary bursts in this event, (2) periodicity of the signals, (3) simultaneity of the elementary bursts at the magnetically conjugate foot-points, and (4) spatial scale of the elementary bursts.

The paper is organized in the following manner: in Section 2, we give a brief overview of the observations; in Sections 3 and 4, we conduct correlation analysis on flare light curves at different wavelengths to determine various time scales and discuss their meanings; and in Section 5 we explore the possibility to spatially map the elementary bursts at a given time scale.

2. Data and Overview

The flare was observed in active region NOAA 8906 during its disk passage on March 16, 2000. A detailed description of instruments and data were given by Qiu *et al.* (2001). To remind readers, we emphasize that, in this event, the Hα -1.3 Å images were taken with a cadence of 100 ms and an image scale of $0.36''$ per pixel. The hard X-ray data were recorded by the pulse count photon detector from the Wide Band Spectrometer (WBS; Yoshimori *et al.*, 1991) on-board *Yohkoh* with a high cadence of 0.125 s in the energy range of 25 – 85 keV. The Hard X-ray Telescope (HXT; Kosugi *et al.*, 1991), a hard X-ray imager on-board *Yohkoh*, observed the flare impulsive phase in four energy channels, L, M1, M2 and H (14 – 23 – 33 – 53 – 93 KeV) with a cadence of 0.5 s. Since this flare is not a strong event, data counts in the H channel are not significantly higher than background, hence we do not use H channel data in this study.

Figure 1 gives a snapshot of the flare morphology at Hα -1.3 Å and HXT M2 channel at the maximum of the flare. Two bright patches, K1 and K2, were

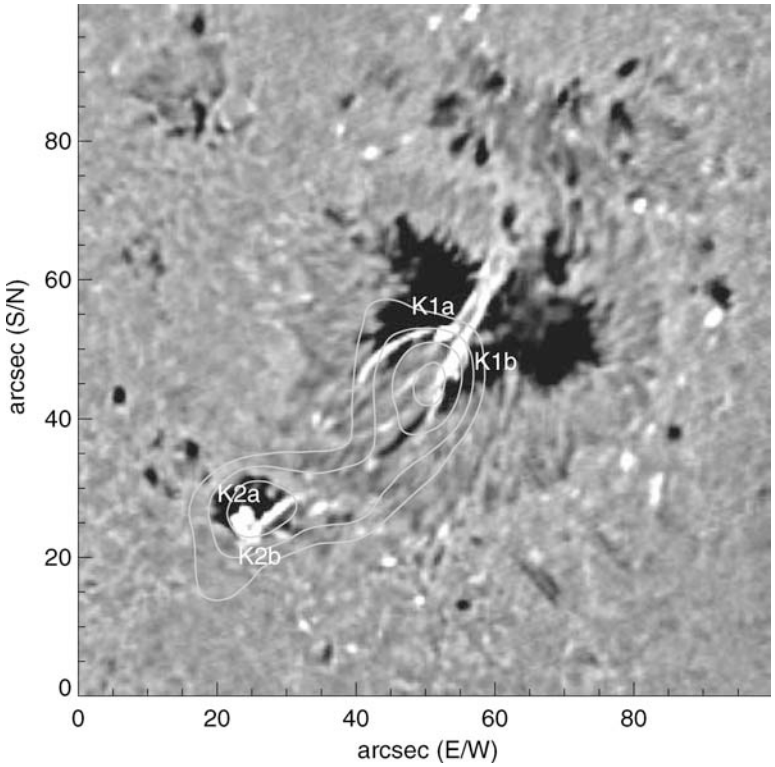

Figure 1. *Greyscale*: snapshot of the flare at its maximum observed at Hα -1.3 Å by BBSO. *Contour*: hard X-ray image from HXT M2 channel. Contour levels are 0.1, 0.2, 0.4, 0.8 of the maximum.

seen throughout the flare, which make two conjugate foot-points of flare loops connecting opposite magnetic polarities (Qiu *et al.*, 2002).

Figure 2 illustrates the light curves of the flare. Light curves in Hα emission are obtained from the spatially resolved sources K1 and K2. Two kinds of Hα light curves are presented, one showing the integrated intensity, or flux, over the flare regions, and the other showing the maximum flare intensity with times. By "maximum", we mean the average over the flare region pixels whose intensity is above 85% of the maximum intensity in the region. The pre-flare emission is subtracted from the Hα light curves. Also presented are hard X-ray light curves from *Yohkoh* HXT 4 channels and WBS pulse count detector at 25 – 85 keV.

Figure 2 shows that the Hα flux light curves bear a great similarity to hard X-ray light curves in the lower energy channels ($\leq$30 keV), and the cross-correlation between Hα flux curves and hard X-ray emission at L and M1 channels is about 90%. This supports the scenario that hard X-ray emission and far wing Hα emission have a common energy release mechanism.

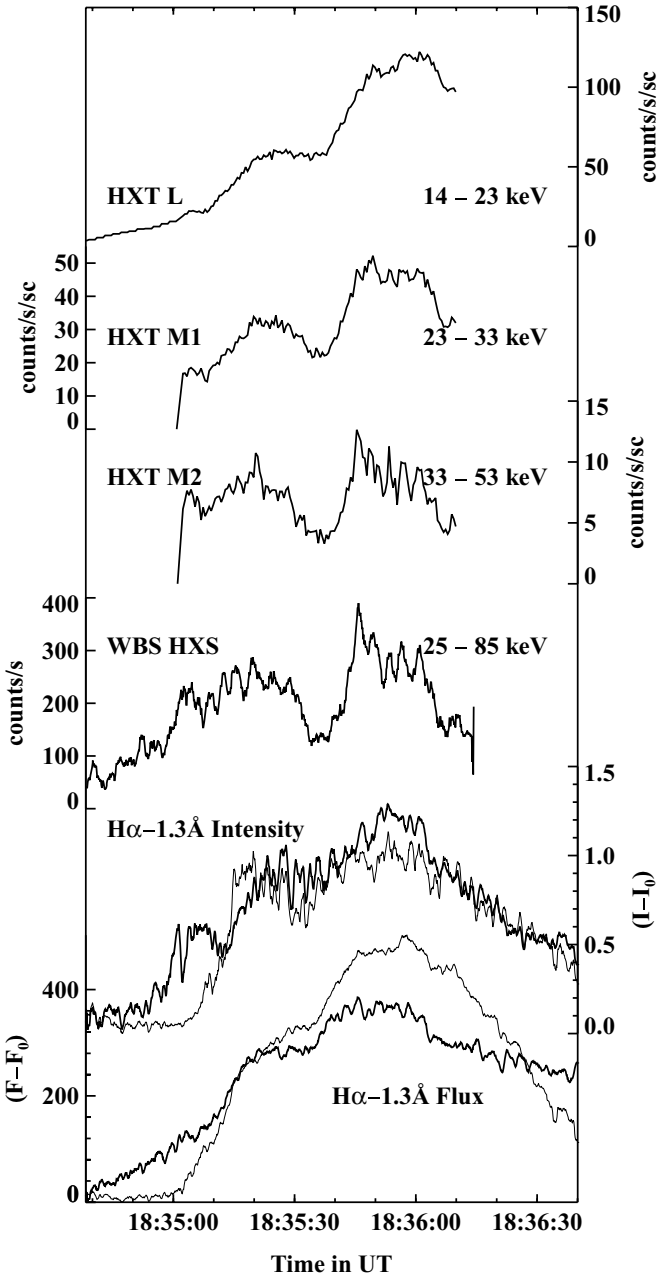

Figure 2. Flare hard X-ray count rates obtained by *Yohkoh* HXT L-M1-M2-H (14 – 23 – 33 – 53 – 93 keV) channels and WBS pulse count detector (25 – 85 keV), and Hα -1.3 Å intensity and flux light curves, with pre-flare emission subtracted, obtained at foot-points K1 (dark) and K2 (grey), respectively.

3. Time Scale of Elementary Bursts

Despite the consensus among solar physicists on the existence of "elementary bursts", there are few papers that give a specific time scale from numerical analysis. Aschwanden *et al.* (1995) is among the very few that quantitatively presented time scales. In this section, we present a practical estimate of the time scale of elementary bursts using available data.

3.1. Hard X-rays from HXT and WBS

The concept of "elementary bursts" usually refers to clusters of hard X-ray and microwave spikes on time scales of several to sub-seconds. In this paper, we follow the traditional concept and first try to determine the fine time scale for this event by using high cadence hard X-ray data. The two hard X-ray instruments, WBS and HXT, are both photon counters, the data counts from which are bound to be contaminated by noises such as statistical errors, hence the nominal temporal resolution of an instrument does not guarantee determination of the shortest time scale which is only limited by the data acquisition rate. Nonetheless, real signals from the sun should be recorded by both instruments as correlated signals, while noisy signals are random and cannot be correlated. Therefore, we can derive the shortest time scale at which the data counts from two hard X-ray observing instruments are well correlated. In this way, we avoid sophisticated error analysis and investigation on the origin of noises, while providing a conservative estimate of the time scale of "elementary bursts". Apparently, the limitation of this method is that sub-second structures, if they exist in this event, cannot be detected by this method, since the time cadence of HXT is 0.5 s.

For a quantitative comparison of hard X-ray data from HXT and WBS, we interpolate the higher cadence (0.125 s) WBS pulse count data, at the energy range of 25 – 85 keV, into the HXT time grids of 0.5 s cadence. Applying a low-pass filter to the data, it is easily found that at >10 s time scale, hard X-ray light curves at various energies are well correlated, with the cross correlation greater than 90% between HXT M2 channel emission (33 – 53 keV) and WBS data (25 – 85 keV). Note that for this study, HXT M2 channel data may be the most appropriate to compare with WBS data, because these two have the closest energy range.

It is difficult in practice to obtain the time scale of correlated fast-varying signals from different instruments by directly applying a high-pass filter to the data. The nature of the high frequency bursts, specifically whether or not they are periodic signals, is not known. Empirically, we consider a few ways to circumvent this problem.

3.1.1. *Method I: Low-Pass Approach*

First, we use a low-pass Fourier filter on both light curves, change the filter cutoff time scale τ from 1 – 8 s, and examine the cross-correlation ρ between HXT and

WBS data versus the cutoff time scale τ. It is expected that a higher cutoff frequency, or a smaller time scale, would produce a lower cross-correlation, because the good correlation is primarily determined by the slow trend. This is illustrated in Figure 3. The left panel of the figure shows the cross-correlation ρ as a function of cutoff time scale τ without applying a time lag in the correlation computation. The middle panel shows the ρ vs. τ plot where ρ is computed as the best correlation with time lags taken into consideration. The right panel in the figure indicates the time lag derived from the maximum correlation computation. From top to bottom, the panels show the correlation of WBS light curve with HXT L, M1 and M2 channel emission respectively. The Figure shows that the cross correlation ρ between WBS data and HXT data from all three channels L-M1-M2 (14 – 23 – 33 – 53 keV) monotonically increases with increasing τ, but at about 4 s, ρ nearly reaches the saturation, beyond which, ρ barely increases any more. The ρ vs. τ relationship, hereafter named as *correlation growth curve*, can be fitted to an exponential function

$$1 - \frac{\rho}{\rho_{\max}} \sim e^{(-\frac{\tau}{\tau_0})}, \tag{1}$$

from which we define the characteristic time scale τ_0 as the correlation time scale. In Figure 3, we over-plot the exponential fit of the ρ vs. τ curve. From the fit, it is determined that $\tau_0 = 1.8, 1.4, 1.3$ s for L, M1 and M2 channels respectively. The right panel in Figure 3 also suggests that there may be a time delay of order 0.5 – 2 s between M1/L channels and WBS 25 – 85 keV emission. But taking into consideration the time lag does not modify the derived time scale τ_0.

3.1.2. *Method II: High-Pass Approach*

In the second method, knowing that signals above 10 s are well correlated, we first remove the slow trend by using a high-pass Fourier filter at 20 s, and then apply the correlation growth curve method to the filtered data, with a changing low-pass filter at times of 1 – 8 s. With this method, there is no longer a good correlation, defined as $\rho > 50\%$, between L channel emission and WBS data, while M1 emission is barely correlated with WBS data and cannot be well described by an exponential relationship. This may be due to the fact that the time scale and correlation at high frequencies are energy dependent. The correlation between WBS and HXT M2 light curves is very good, and from the fit of ρ vs. τ between M2 and WBS data, $\tau_0 = 2.3$ s.

3.1.3. *Method III: Slow-Trend Envelope*

The third method is to subtract from the original light curve a slow-trend envelope which is determined by a smooth curve connecting the local minima (Aschwanden *et al.*, 1997). The time of a local minimum $t_{\min}$ is found when $\frac{\partial I}{\partial t} < \epsilon$ and $\frac{\partial^2 I}{\partial t^2} > 0$ at $t_{\min}$, where I is the light curve, and ϵ is a small number, here taken as 0.5 times the standard deviation of $\frac{\partial I}{\partial t}$. This way, only the fast-varying signals are reserved. With the high-pass Fourier filter method (method II), the residual signals can be

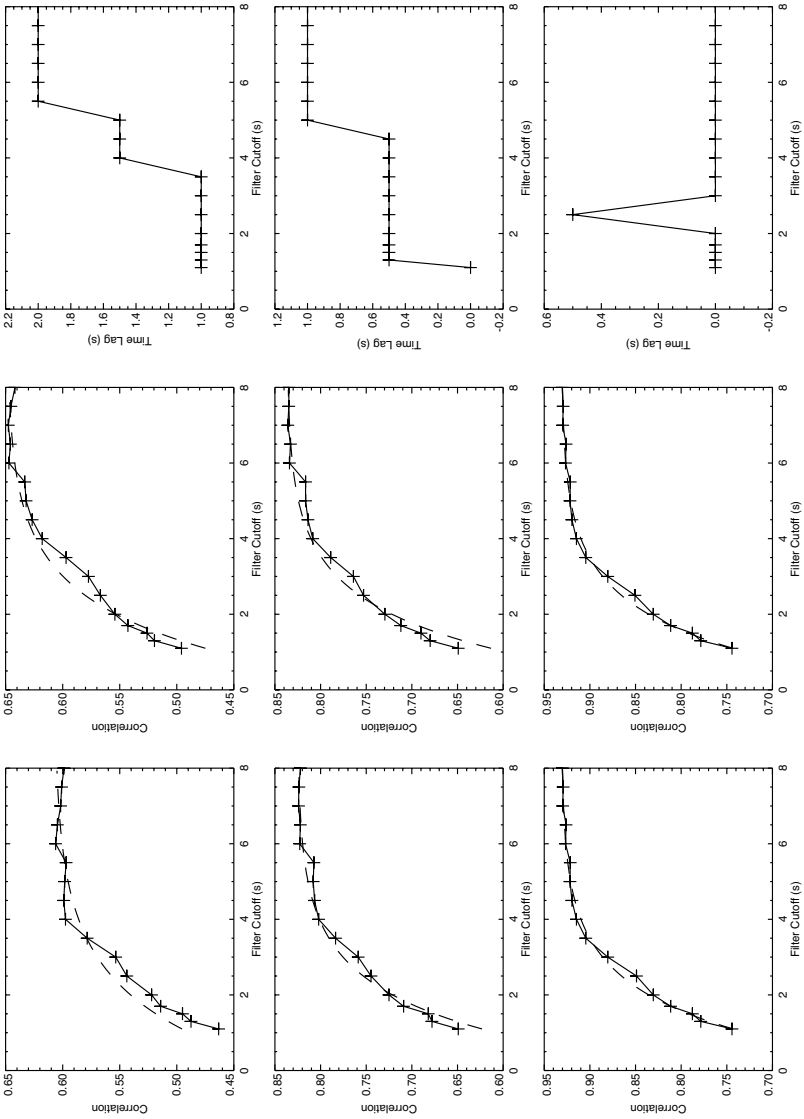

Figure 3. Left and middle: cross-correlation between hard X-ray count rates obtained by WBS HXS detector and by HXT L (*upper panel*), M1 (*middle panel*), and M2 (*lower panel*) channels as a function of the cut-off time of the high-pass filter (see text). *Left/middle panels* show cases without/with a time lag applied to the cross-correlation calculation. *The dashed curves* show the fit to an exponential *correlation growth curve* (see text). *Right*: the time lag obtained in computing the maximum cross-correlation.

TABLE I

τ_0 Determined between WBS (25 – 85 keV) and HXT (L-M1-M2 channel) light curves.

Method	L	M1	M2
I	1.8	1.4	1.3
II	–	–	2.3
III	–	–	2.2

either positive or negative, which represent fluctuations over a slow-varying average light curve. Whereas the envelope method yields only positive fast-varying signals which are superposed on the slow trend time profile. The determination of the slow trend envelope is also dependent on the time scale τ, and the correlation between the residual high frequency signals is derived as ρ. By fitting the ρ vs. τ plot to Equation (1), we find $\tau_0 = 2.2$ s for M2 channel, whereas results for L and M1 channels are not reliable.

3.1.4. *Short Summary*

In Table I, we list the time scales determined with the above three methods by fitting the correlation growth curves for hard X-ray emissions at WBS and HXT L-M1-M2 channels. To be consistent, we only use the results from all three methods for M2 channel data. Taking an average of the obtained τ_0 from the above three methods, we find that $\tau_0 = 1.9 \pm 0.5$ s is a conservative time scale of elementary bursts in this event, empirically determined through cross-correlation study. Here the cited error reflects the variation of τ_0 determined by the three methods.

We have two comments on this result. First, the cadence of WBS and HXT observations is 0.125 s and 0.5 s respectively. From both instruments, fine temporal structures at time scales much shorter than 2 s are visible, some of which are probably real signals. The value of 2 s we have determined through cross-correlation analysis between signals from the two instruments is a conservative value serving as an upper-limit of experimentally determined shortest time scale. Second, in this paper, we do not investigate time lags between different energy channels, but the correlation analysis with method I shows that, on average, L (14 – 23 keV) and M1 (23 – 33 keV) emissions lag the WBS (25 – 85 keV) emission by 1.4 and 0.7 s, respectively (Figure 3). These time lags are obtained between fast-varying signals. They likely reflect the Time-Of-Flight (TOF; Aschwanden *et al.*, 1996 and references therein) of non-thermal electrons precipitating from the loop top to foot-points, and higher energy electrons arrive at the foot-points earlier than lower energy electrons. Assuming that the average electron energy is about twice the photon energy (Nitta and Kosugi, 1986), the amount of average time lags with respect to energies would yield the loop length of about 2×10^9 cm, comparable with the distance between the two foot-points (Figure 1). With methods II and III, the time

lags between L/M1 and WBS in the range of tens of seconds are not deemed as meaningful. All three methods yield a close to zero time lag between M2 and WBS data, hence we regard that there is not a time lag between the two detectors, which probably receive emission by same electrons.

3.2. Hα AND HARD X-RAYS

In this section, we explore the cross-correlation between Hα and hard X-ray light curves at different energies, in order to check whether the temporal structures of elementary bursts can be verified at optical wavelengths. Since Hα data have good spatial resolution, if the fast-varying "elementary bursts" are found in Hα wavelengths as correlated with hard X-rays, it is logical to search for spatial fragmentation from high resolution Hα images. The cadence of Hα observations of this flare is about 0.1 s, and we interpolate the Hα light curves into the HXT time grids of 0.5 s cadence.

In doing this, we are aware that there can be insurmountable difficulties. First, Hα data were obtained by ground-based instruments with seeing effects hard to separate from real signals. Second, due to heating, ionization, and complicated radiative transfer time scales of the lower atmosphere, there is not already established knowledge on how fast lower atmosphere Hα emission can be correlated with hard X-ray emission, which is produced by instantaneous Coulomb collision of injected electrons with the ion target in the upper chromosphere. Third, as we can see from Figure 2, on larger time scales, e.g., of >10 s, Hα flux light curve is better correlated with low energy hard X-ray emission. While fast varying structures are more evident in Hα maximum intensity light curves (i.e., the light curve of the average intensity over the flare region pixels whose intensity is above 85% of the maximum intensity in the region), similar to hard X-ray higher energy emission. Physically, it is not clear which type of Hα light curves should be employed for the cross-correlation study. In this paper, we apply the correlation growth curve methods to both types of Hα light curves to derive time scales of cross correlation between Hα emission and hard X-rays at different energies.

The use of the peak intensity light curves is based on the assumption that at a given duration of the emission peak, a package of electrons is deposited at a single location – the upper-limit of its detectable size being dependent on instrument resolution – to produce instantaneous strongest emission at the site, while emission produced during the preceding peak at possibly a different location has decayed sufficiently fast. On the other hand, the use of the integrated intensity light curves is based on the assumption that at a given time scale, non-thermal electrons are not deposited at a specific site, but are spread at various locations embedded within the flare region, so that the integrated flux containing the information of the flaring area as well, rather than the maximum intensity, would compare better with hard X-rays.

We first investigate correlation between Hα flux and HXT L, M1 and M2 channel emissions using the same three methods. The results are listed in Table II. From

TABLE II

τ_0 determined between Hα and HXT (L-M1-M2 channel) light curves.

Method	L	M1	M2
I	3.5	4.2	–
II	1.7	–	–
III	–	–	–

method I, hard X-ray emissions from L and M1 channels exhibit reasonable correlation (>80%) with Hα flux with a zero time lag and similar ρ vs. τ plots, from which τ_0 is determined to be 3.5 and 4.2 s, respectively. From method II, Hα < 10 s signals are only correlated with L channel emission with $\tau_0 = 1.7$ s. Results from method III are not stable hence discarded. Comparing the results from the first two methods, it is not evident that there is correlation between Hα emission and hard X-ray emission in other than L channel at time scales of order a few seconds. We hence adopt the values determined by the first two methods for only the *L* channel emission, and on average $\tau_0 = 2.6 \pm 1.3$ s. It is also found that there is not a time lag between L channel hard X-ray emission and Hα flux intensity.

Then we compare hard X-rays with Hα maximum intensity light curves, derived at two foot-points respectively. For neither of the kernels, we can find evident and unambiguous correlation between Hα signals and hard X-ray emission at time scales smaller than 10 s.

The above results can be understood in the following ways. First, the correlation between Hα emission with hard X-ray fast-varying signals only in L channel (14 – 23 keV) indicates that the lower energy electrons play the primary role in bulk heating the lower atmosphere, even at the time scale of 2 – 3 s. Second, the generally better correlation of hard X-rays with Hα flux may suggest that "elementary bursts" at 2 – 3 s time scale is a result of non-thermal electron precipitation in extended areas rather than that a package of electrons precipitate at a single location. However, we cannot be too certain about this, because the atmospheric heating and cooling time scale may contaminate the correlation study, and for the Hα maximum intensity light curve, seeing effects may be seriously exaggerated such that we do not obtain a positive result.

Additionally, the power spectrum of neither hard X-ray nor Hα time profile indicates existence of any dominant frequency or frequency range apart from the zeroth and first powers. So emission at neither wavelength is periodic. This conclusion is consistent with the results by Kiplinger *et al.* (1983, 1988) and Aschwanden *et al.* (1993, 1995, 1998). But the same cannot be generalized to all flares, since Wang *et al.* (2000) have found a dominant time scale of 0.3 – 0.7 s. Therefore, for different flares, the mechanisms of elementary bursts may fundamentally differ.

4. Hα Emissions at Magnetic Conjugates

Analysis of hard X-ray observations as done in Section 3.1 is limited by the HXT cadence (0.5 s) which cannot reveal time scales shorter than 1 s, if any. Nevertheless, an alternative way to explore the limit is to derive the minimum time scale at which Hα emissions at two foot-points correlate. The method is valid if the following assumptions hold. First, accelerated electrons travel along the magnetic field lines symmetrically toward the conjugate foot-points. Second, the time of flight is ignorable. And last, the atmosphere heating and cooling time scales at the two sites are the same, and are shorter than 1 s. The first two assumptions can be reasonably regarded as true based on the flare morphology. For example, the flight time of an electron with 10 keV energy over 10^9cm distance is less than 0.2 s. Whether the third assumption holds can be tested by examining the time scale of the connectivity through Hα emission.

As seen in Figure 1, two bright patches, or flare kernels, K1 and K2, are observed throughout the flare evolution. Soft X-ray and EUV images suggest that they are conjugate foot-points connected by magnetic field lines, along which heat flux or electron beams propagate to the chromosphere. For light curves of either the maximum intensity or the flux, the cross-correlation between emissions from the two kernels is larger than 90%, indicating a generally good coincidence in the flare emission at the two kernels. We then employ the correlation growth curve methods described above to study correlation between fast-varying signals. Because the third method is not stable for Hα emission, we only use the first two methods to obtain the correlation growth curves. As an example, Figure 4 shows the result with the first method. The exponential fit to the correlation growth curve from the two methods yield $\tau_0 = 2.7$, 1.3 s respectively (Table III), both with a zero time lag. As an average of the two methods, $\tau_0 = 2.0 \pm 1.0$ s, at which Hα flux from the two foot-points correlates. We also examine correlation of the maximum intensity between two foot-points. This gives $\tau_0 = 2.2$, 1.5 s (Table III), hence on average $\tau_0 = 1.9 \pm 0.5$ s, which is comparable with the flux time scale. So here we see that although we do not find correlation between hard X-ray and Hα maximum intensities, Hα maximum intensities at the two foot-points are correlated with each other at up to 2 s time scale.

Note that although $\tau_0 \approx 2$ s is found to be the characteristic time scale for the spatial connectivity, this is a conservative upper limit. Looking at Figure 4, if we

TABLE III

τ_0 between K1 and K2 Hα light curves.

Method	Flux	Intensity
I	2.7	2.2
II	1.3	1.5

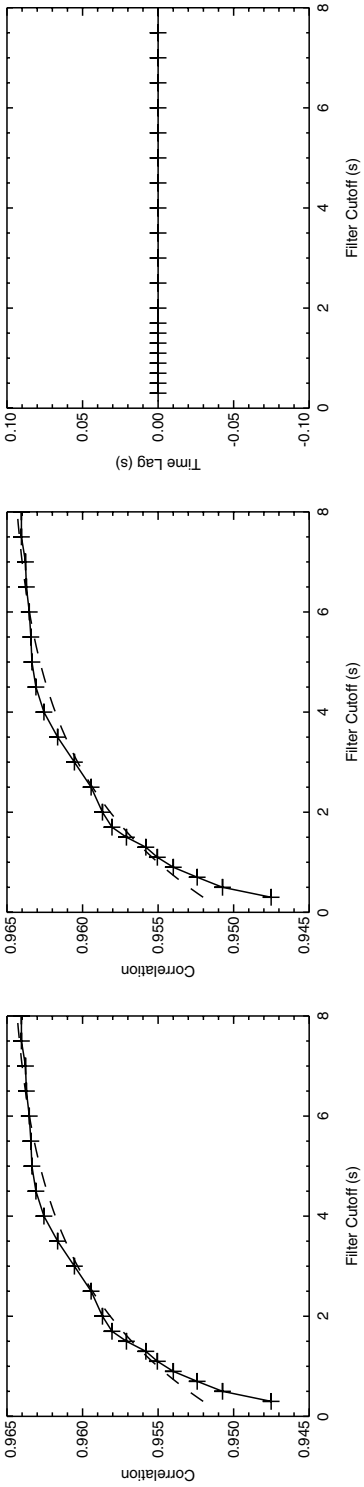

Figure 4. Similar to Figure 3, but for comparing Hα flux light curves obtained at K1 and K2 kernels.

regard that 50% cross-correlation indicates a significant correlation, then emissions at the two foot-points may actually correlate at below 1 s. For this to be discernible in spatially resolved Hα observations, it requires that ionization, heating, and cooling of the lower chromosphere are sufficiently fast.

5. Spatial Scales of Elementary Bursts

Attempt to map elementary bursts is a challenging task. Combining seeing-free hard X-ray observations by space instruments and high cadence and high resolution imaging observations by BBSO, we try to approach this problem by studying the spatial evolution of Hα emission at the times of hard X-ray spikes.

For this purpose, we first determine the times of hard X-ray peaks, at varying time scales from 0.5 to 10 seconds, in the hard X-ray light curves. Then in Hα images, we locate the brightest pixel in the Hα kernels, specifically, K1a, K1b, K2a and K2b (see Figure 1) as can be resolved from the morphological evolution, at the times of the hard X-ray peaks. We then compute the average spatial shift of the brightest Hα loci between successive hard X-ray peaks. Figure 5 illustrates the times of hard X-ray peaks on the time scale of 3 s, and the displacement of the brightest Hα loci between successive hard X-ray peaks. This can be done given various time scales, and Figure 6 shows the average shift against the average time interval between successive hard X-ray peaks. It is seen that, from the shortest time scale available (here 0.5 s) to up to about 3 s, the average spatial displacement is in the order of $0.4 \pm 0.4''$ for K1a and $0.5 \pm 0.5''$ for K1b, and with the time interval increasing to be above 3 s, the amount of the spatial shift is monotonically increasing so as to join the regime of the large scale smooth "motion" as reported in an earlier paper by Qiu *et al.* (2002). For the case of K2a and K2b, which are compact sources inside a pore, the amount of the average displacement is smaller by a factor of 2 to 3, and towards larger time scales above 3 s, the average displacement remains small.

The plot in Figure 6 suggests that 2 – 3 s is a critical time-scale. On timescales above 3 s, the average speed of the brightest Hα loci within kernels K1a and K1b is about 40 km s^{-1}, consistent with the large-scale "sweeping" motion at the velocity ranging from $\approx$20 – 100 km s^{-1} (Qiu *et al.*, 2002). Here the term "motion" does not mean a real motion of the flare foot-point, but rather the changing locations of excitation at the chromosphere. On shorter time scales from 0.5 to 3 s, we note that the smallest spatial scales determined are all close to or below the CCD pixel size ($\approx 0.4''$/pixel), which raises the question whether the time scale of 2 – 3 s and the spatial scale related to it are physically meaningful.

We may assume that 2 – 3 s is a physically meaningful cutoff timescale for the macroscopic reconnection in an organized manner. In this case, given the macroscopic average velocity of 20 – 100 km s^{-1}, at 2 – 3 s, the upper-limit of the spatial scale is about $0.4''$, which is the same as observationally determined from Figure 6.

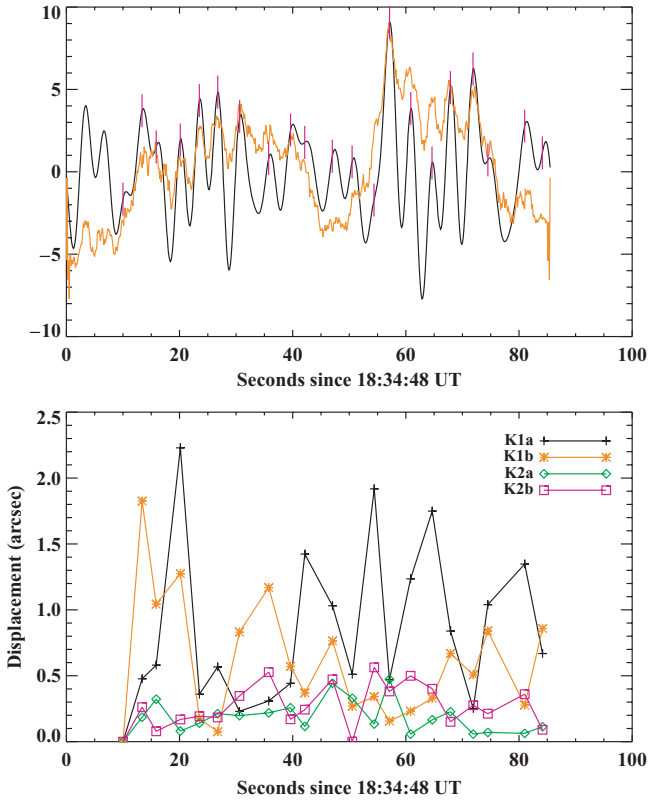

Figure 5. Upper panel: the original (*orange*) and high-pass filtered (*dark*) hard X-ray count rates by WBS HXS detectors. In this figure, the high-pass cut-off is 3 s. Both hard X-ray light curves are shown in arbitrary units. *Purple vertical bars* indicate identified elementary bursts. *Lower*: displacement of the locations of Hα peak emission at various flare kernels between successive hard X-ray peaks.

Therefore, the value of $0.4''$ is likely the critical spatial scale dividing the macroscopic and microscopic regimes, though this statement is not conclusive as this value is too close to the image scale of Hα observations.

We discuss several known mechanisms that may incorporate the time and spatial scales derived above. First, we consider magnetic reconnection between single flux tubes. The characteristic size of a single flux tube is $L \approx V_{\rm A}\tau$, where $V_{\rm A}$ is the Alfven speed, and τ is the timescale of elementary bursts. The typical coronal Alfven speed is of order 10^3 km s^{-1}. Given $\tau \approx 2 - 3$ s, L in the corona is about $2-3\times10^3$ km. Downward into the chromosphere, because the plasma density increases faster than the magnetic fields, $V_{\rm A}$ can be smaller by an order of magnitude. Therefore, at $2-3$ s, the spatial scale is about half an arc-second, comparable to the spatial scale experimentally determined in above paragraphs. The chromospheric spatial scale may be also estimated in a slightly different way. Since the flux tube

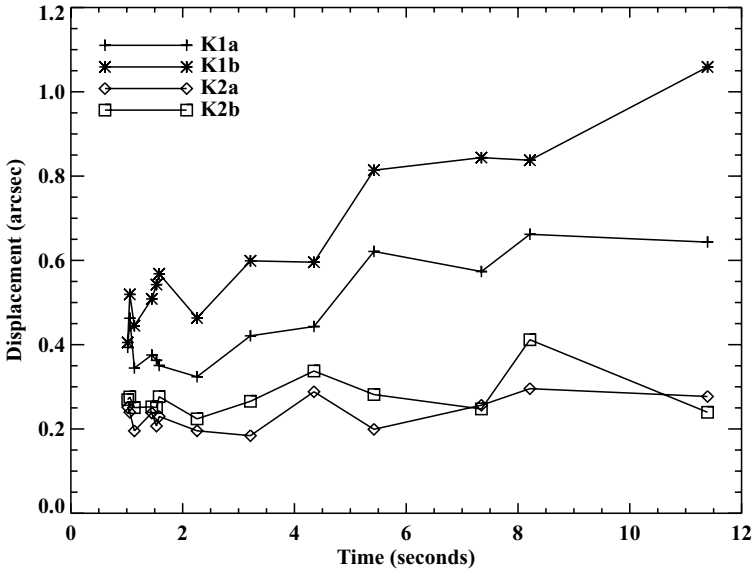

Figure 6. Mean displacement of the locations of Hα peak emission at various flare kernels between successive hard X-ray peaks versus the average time intervals of hard X-ray bursts.

flux is conserved from the corona to the lower atmosphere during the reconnection timescale, there is $B_c L_c^2 = B_l L_l^2$, where the items in the lefthand and righthand sides of the equation refer to the corona and the lower atmosphere, respectively. This relation is reduced to $L_l = L_c (B_c/B_l)^{0.5}$, where $L_c \approx 2 - 3 \times 10^3$ km. As the coronal magnetic field strength is typically about 1 – 2 orders of magnitude smaller than B in the lower-atmosphere, it is also seen that the characteristic size of a single flux tube in the chromosphere be several hundred kms. In other words, on the timescales of 2 – 3 s, the regime of large-scale reconnection in an organized manner turns to the regime governed by the size of a single flux tube, which is about a fraction of an arc-second.

On the other hand, a tearing-mode instability may occur inside the current sheet in the corona, forming magnetic islands. The time scale of the instability τ_t is estimated to be between $\tau_D^{3/5} \tau_A^{2/5}$ and $\tau_D^{1/2} \tau_A^{1/2}$, depending on the wavelength of the disturbance, where $\tau_D = l^2/\eta$ is the resistive diffusion time scale, and $\tau_A = l/v_A$ is the Alfven transit time (Priest, 1982). l is the characteristic width of the current sheet, η is the resistivity, and v_A is the Alfven speed at the current sheet. Given v_A of order 10^6 m s^{-1}, and η of order 1 m^2 s^{-1} in solar corona condition, if $\tau_t \approx 2 - 3$ s as observed, it requires $l \approx 50 - 200$ m. Given an anomalous resistivity η_a of order 100η, then $l \approx 300 - 1000$ m. The size of magnetic islands is believed to be a few orders of magnitude greater than l, which is likely close to the observed spatial scale thus hard to be distinguished from the scenario of reconnection between individual flux tubes without additional information.

6. Summary

In this paper, we explore the time and spatial properties of "elementary bursts" using high cadence hard X-ray and Hα observations. Because of practical difficulties in identifying fine structures in data from a single instrument, we have applied cross-correlation analysis to signals observed by different instruments at various wavelengths, and derived the characteristic time scale from the correlation growth curve. The results of this study are summarized below.

We find that at 2 s, hard X-ray emissions recorded by different instruments are correlated, hence 2 s is taken as a conservative estimate, or upper-limit, of the time scale of hard X-ray elementary bursts in this event.

At a similar time scale of 2 – 3 s, we find that the light curve of integrated flux at Hα $-$ 1.3 Å is correlated with hard X-ray low energy emission at $<$30 keV. Correlation is not found in fast-varying structures with other types of Hα light curves or with higher energy X-rays. This result suggests that the "elementary" Hα emission is mostly produced by lower-energy electrons, and the electron "package" at $\approx$2 – 3 s time scale is injected over a diffused region rather than concentrated at one location.

The characteristic fine time scale at which emissions from two conjugate foot-points are significantly correlated, or in other words, the simultaneity of energy deposition at conjugate foot-points, is accurate at up to 2 s, though there is an indication of sub-second scales.

In this event, emission recorded at none of the observing wavelengths suggests existence of periodicity.

The high cadence and high resolution BBSO Hα off-band observations also provide opportunities to explore the spatial structure of elementary bursts. We find the mean shift of the brightest Hα loci between successive hard X-ray spikes at time scales above 2 s increases with the time interval, with an average speed of about 40 km s^{-1}. The average spatial shift on time scales from 0.5 to 2 – 3 s is about half an arc-second, very close to the spatial resolution of the observations. These scales may reflect the characteristic scales of single flux tubes, which are marginally resolvable with the existing imaging capabilities. Even smaller scales that govern the microscopic physics of magnetic reconnection are beyond the resolving power of the observing instruments.

Acknowledgements

We are grateful to the BBSO staff and *Yohkoh* team for the data support. This work is supported by NASA grants NNG0-4GG21G and NNG0-6GA37G and NSF grant ATM-0603789.

References

Aschwanden, M.J.: 2002, *Particle Acceleration and Kinematics in Solar Flares, A Synthesis of Recent Observations and Theoretical Concepts*, Kluwer Academic Publishers, Dordrecht, Holland.

Aschwanden, M.J., Benz, A.O., Dennis, B.R., and Schwartz, R.A.: 1995, *Astrophys. J.* **455**, 347.

Aschwanden, M.J., Benz, A.O., and Schwartz, R.A.: 1993, *Astrophys. J.* **417**, 790.

Aschwanden, M.J., Kliem, B., Schwarz, U., Kurths, J., Dennis, B.R., and Schwartz, R.A.: 1998, *Astrophys. J.* **505**, 941.

Aschwanden, M.J., Kosugi, T., Hudson, H.S., Wills, M.J., and Schwartz, R.A.: 1996, *Astrophys. J.* **468**, 398.

Aschwanden, M.J., Schwartz, R.A., and Alt, D.M.: 1995, *Astrophys. J.* **447**, 923.

Bastian, T.S. and Vlahos, L.: 1997, in G. Trottet (ed.), *Coronal Physics from Radio and Space Observations*, Springer Verlag, Berlin, p. 68.

Benka, S.G. and Holman, G.D.: 1994, *Astrophys. J.* **435**, 469.

de Jager, C. and de Jonge, G.: 1978, *Solar Phys.* **64**, 135.

Ding, M.D., Qiu, J., Wang, H., and Goode, P.R.: 2001, *Astrophys. J.* **552**, 340.

Furth, H.P., Killeen, J., and Rosenbluth, M.N.: 1963, *Phys. Fluids* **6**, 459.

Holman, G.D.: 1985, *Astrophys. J.* **293**, 584.

Hoyng, P., van Beek, H.F., and Brown, J.C.: 1976, *Solar Phys.* **48**, 197.

Kaufmann, P., Strauss, F.M., Laporte, C., and Opher, R.: 1980, *Astron. Astrophys.* **87**, 58.

Kaufmann, P., Correia, E., Costa, J.E.R., Dennis, B.R., Hurford, G.J., and Brown, J.C.: 1984, *Solar Phys.* **91**, 359.

Kaufmann, P. *et al.*: 2001, *Astrophys. J.* **548**, L95.

Kiplinger, A.L., Dennis, B.R., Emslie, A.G., Frost, K.J., and Orwig, L.E.: 1983, *Astrophys. J.* **265**, L99.

Kiplinger, A.L., Dennis, B.R., Orwig, L.E., and Chen, P.C.: 1988, in R.C. Canfield and B.R. Dennis (eds.), *Max 1991: Flare Research at the Next Solar Maximum Workshop 1: Scientific Objectives, NASA-TM-101259,* p. 214.

Kliem, B., Karlick, M., and Benz, A.O.: 2000, *Astron. Astrophys.* **360**, 715.

Kosugi, T. *et al.*: 1991, *Solar Phys.* **136**, 17.

Kurt, V.G., Akimov, V.V., Hagyard, M.J., and Hathaway, D.H.: 2000, in R. Ramaty and N. Mandzhavidze (eds.), *High Energy Solar Physics: Anticipating HESSI, Astron. Soc. Pacific. Conf. Ser.* **206**, 426.

LaRosa, T.N. and Moore, R.L.: 1993, *Astrophys. J.* **418**, 912.

Lu, E.T. and Hamilton, R.J.: 1991, *Astrophys. J.* **380**, L89.

Nitta, N. and Kosugi, T.: 1986, *Solar Phys.* **105**, 73.

Ogawara, Y. *et al.*: 1991, *Solar Phys.* **136**, 1.

Parker, E.N.: 1989, *Solar Phys.* **121**, 271.

Priest, E.R.: 1982, *Solar Magnetohydrodynamics*, D. Reidel Publishing Company, Dordrecht, Holland.

Qiu, J. *et al.*: 2001, *Astrophys. J.* **554**, 445.

Qiu, J., Lee, J., Gary, D.E., and Wang, H.: 2002, *Astrophys. J.* **565**, 1335.

Sakao, T.: 1994, Ph.D. thesis, University of Tokyo.

Sato, J., Kosugi, T., and Makishima, K.: 1999, *Publ. Astron. Soc. Japan* **51**, 127.

Sturrock, P.A., Kaufman, P., Moore, R.L., and Smith, D.F.: 1984, *Solar Phys.* **94**, 341.

Švestka, Z.: 1976, *Solar Flares*, D. Reidel Publishing Company, Dordrecht, Holland.

Švestka, Z. and Cliver, E.W.: 1992, in Z. Švestka, B.V. Jackson, and M.E. Machado (eds.), *Eruptive Solar Flares*, Springer-Verlag, Berlin, p.1.

Trottet, G. *et al.*: 2000, *Astron. Astrophys.* **356**, 1067.

van Beek, H.F., de Feiter, L.D., and de Jager, C.: 1974, in M.Z. Rycroft and R.D. Reasonberg (eds.), *Space Research XIV: Proceedings of the Sixteenth Plenary Meeting,*, Akademie-Verlag, Berlin, p. 447.

van Beek, H.F., de Feiter, L.D., and de Jager, C.: 1976, in M. Rycroft (ed.), *Space Research XVI: Proceedings of the Open Meetings of Working Groups on Physical Sciences*, Akademie-Verlag, Berlin, p. 819.

Wang, H., Qiu, J., Denker, C., Spirock, T., Chen, H., and Goode, P.R.: 2000, *Astrophys. J.* **542**, 1080.

Wang, H. and Qiu, J.: 2002, *Astrophys. J.* **568**, 408.

Yoshimori, M. *et al.*: 1991, *Solar Phys.* **136**, 69.